Molecular Therapy
Methods & Clinical Development
Original Article

Evaluation of the loading capacity and patterns of packaged DNA in AAV genomes of different sizes using long-read sequencing

Mitsuki Kosaka,[1] Ai Fujita Sajiki,[1,2] Kosuke Fujita,[1] Kazuhisa Yamada,[1] Kenichi Kawano,[1,3] Kiichi Hirazawa,[1] Tsuyoshi Matsuno,[1] Masahiko Takada,[4] Nobuhiro Shimozawa,[5] Ken-ichi Inoue,[4] Kenya Yuki,[1] and Koji M. Nishiguchi[1]

[1]Department of Ophthalmology, Nagoya University Graduate School of Medicine, Nagoya, Aichi 466-8550, Japan; [2]Division for Advanced Medical Research, Center for Research of Laboratory Animals and Medical Research Engineering, Nagoya University Graduate School of Medicine, Nagoya, Aichi 466-8550, Japan; [3]Department of Ophthalmology, Yokkaichi Municipal Hospital, Yokkaichi, Mie 510-8567, Japan; [4]Systems Neuroscience Section, Center for the Evolutionary Origins of Human Behavior, Kyoto University, Inuyama, Aichi 484-8506, Japan; [5]Tsukuba Primate Research Center, National Institutes of Biomedical Innovation, Health and Nutrition, Tsukuba, Ibaraki 305-0843, Japan

The loading capacity of adeno-associated virus (AAV) vectors is reportedly 4.7–5.0 kb, which limits the size of genes that can be treated with gene therapy. However, the effects of oversized genomes on the integrity of packaged AAV genomes are poorly understood. Herein, nanopore long-read sequencing was used to evaluate genomic integrity in AAV vectors harboring genomes of various sizes. AAV had a reduced proportion of full-length genomes at a vector length of 4.9 kb, which declined rapidly between 4.9 and 5.0 kb. This was mainly attributable to defects in genome packaging rather than genome synthesis. Furthermore, the pattern of packaged DNA was unique to the arrangement of the components of the oversized genome. However, an 86.3% reduction in the proportion of full-length genomes (4.7 vs. 5.0 kb) was not consistent with the retained expression of the reporter gene in the mouse retina. This discrepancy might be partially attributable to the preferential inclusion of the region containing the reporter gene. These results highlight the utility of long-read sequencing in assessing the genomic integrity and design of AAV vectors, as the pattern of packaged genomes appears to be unique to each vector, particularly for oversized AAV genomes.

INTRODUCTION

Adeno-associated virus (AAV) vectors have been widely explored to complement the function of defective genes by introducing a normal copy of the full-length cDNA into diseased cells with loss-of-function mutations in rare forms of inherited disease.[1] Recently, AAV vectors have been used to deliver therapeutic genes in more common intractable diseases.[2,3] However, the genomic packaging limit for AAV capsids is 4.9–5.2 kb,[4–7] which limits the design of vectors for therapeutic transgene delivery.[8] Understanding the packaging capacity of AAV vectors is necessary for their effective use in gene therapy. The cargo capacity of AAV vectors has been assessed by western blotting, electrophoresis, chromatography, and *in vitro* expression.[4–6] In particular, strand-specific dot-blot hybridization shows that vectors exceeding 5.2 kb harbor AAV genomes of heterogeneous lengths or truncated at the 5′ end.[4] However, this analysis only confirms the site where the hybridization probe is placed and does not assess whether and how the genome is cleaved. To date, little is known about the effects of oversized AAV genomes on replication and packaging, especially the patterns of defective AAV genomes.

Recently, long-read sequencing, which allows us to examine the entire AAV genome without genome amplification, has been applied to study the AAV genome.[9] Conventional short-read sequencing can be used to qualitatively assess small fragments of the AAV genome after PCR amplification.[10,11] However, short-read sequencing is unsuitable for studying the effects of oversized AAVs when quantitative comparisons between different regions within the genome are needed. To our knowledge, no previous studies have focused on the genome status of AAV vectors using long-read sequencing.

The nanopore system is a commonly used long-read sequencing platform due to its simple operation system and cost-effectiveness.[12–14] Importantly, the nanopore system allows us to rapidly obtain longer sequence information of up to 4.2 Mb without genome amplification.[14,15] Thus, this platform has been used to identify pathogenic bacteria,[16–19] evaluate the accuracy and efficiency of genome editing,[9] and analyze the COVID-19 genome.[20,21]

In this study, nanopore long-read sequencing was used to evaluate the integrity of AAV genomes of different sizes. In addition, the

Received 1 October 2024; accepted 16 April 2025;
https://doi.org/10.1016/j.omtm.2025.101474.

Correspondence: Ai Fujita Sajiki, MD, PhD, Department of Ophthalmology, Nagoya University Graduate School of Medicine, 65 Tsurumai-cho, Showa-ku, Nagoya, Aichi 466-8550, Japan.
E-mail: fujita.ai@med.nagoya-u.ac.jp

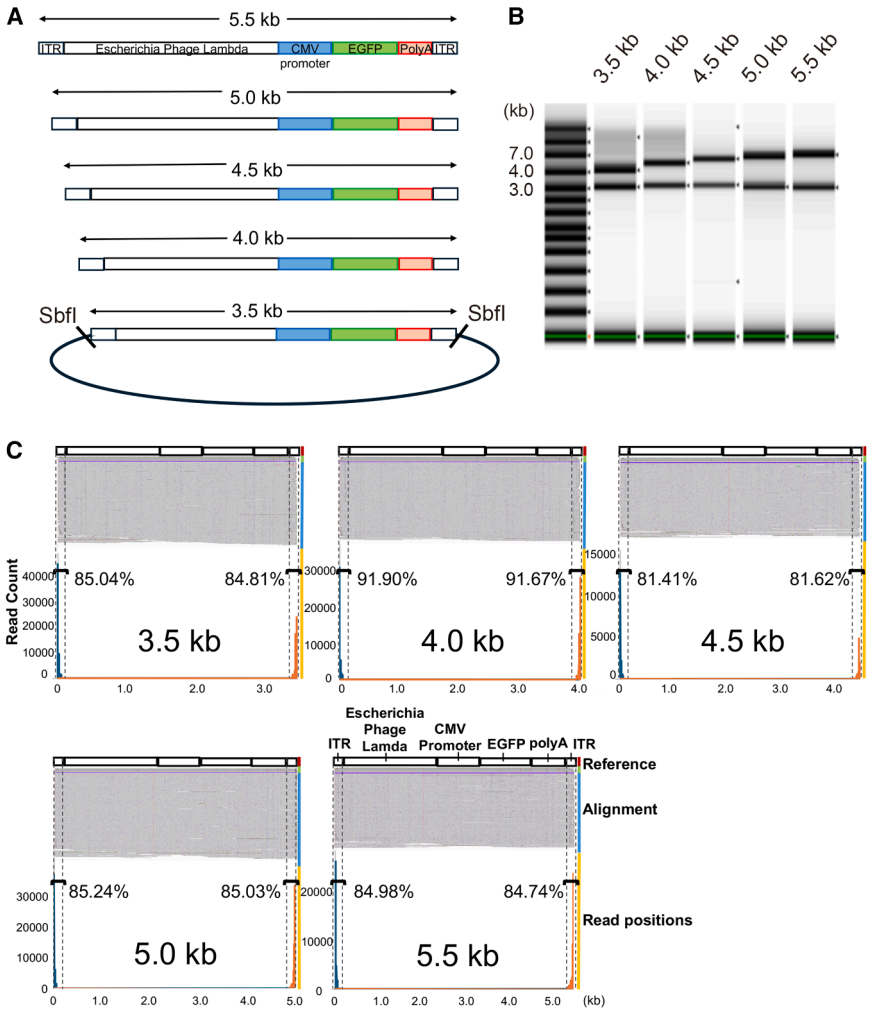

Figure 1. Vectors of different sizes

Vectors of different sizes were constructed, and each plasmid-encoded vector was evaluated using nanopore sequencing. (A) The structure of the 3.5–5.5 kb AAV8 genome. The vectors contained a fixed-size EGFP expression cassette and lambda phage DNA of various lengths to alter the length of the vector. (B) The plasmid-encoded vectors of different sizes were quantified and confirmed using TapeStation. (C) The plasmids (3.5–5.5 kb) were analyzed using nanopore sequencing. The AAV genome components are displayed above the sequence alignment. Each representative read alignment is displayed in IGV; nucleotides that match the reference sequence are shown in gray. The graph below each read alignment shows the count of the start and end positions of the reads; the start positions are indicated in blue, and the end positions are indicated in orange. The percentages of start and end positions of each read inside the ITRs are shown in the graph.

effects of oversized AAV genomes on the expression of the reporter gene embedded within AAV vectors were examined *in vivo*.

RESULTS

Evaluation of plasmids used for AAV production

AAV plasmids with different genome sizes were created to assess the integrity of the packaged AAV genome. First, the size of the AAV genome containing the enhanced green fluorescent protein (EGFP) expression cassette was adjusted with spacer lambda phage sequences of various sizes to generate 3.5, 4.0, 4.5, 5.0, and 5.5 kb vectors (Figure 1A). The genome sizes of these plasmids were confirmed using TapeStation. The bands were consistent with the sizes of the corresponding AAV genomes (Figure 1B).

The integrity of these plasmid genomes was analyzed using long-read sequencing with the nanopore platform (Figure 1C). The plasmid-encoded vectors had start and end points within the inverted terminal repeats (ITRs) with a percentage of approximately 80%–90%, and no obvious differences were observed between the vectors of different sizes (Figure 1C and Table S1).

Evaluation of the DNA integrity of AAV vectors

Qualitative analysis with agarose gel electrophoresis revealed single clear bands at the expected AAV genome sizes of 3.5, 4.0, 4.5, 4.6, 4.7, 4.8, and 4.9 kb but not at 5.0 or 5.5 kb, where multiple smaller-sized bands formed a smear (Figure 2A). The AAV genome was qualitatively evaluated to confirm its size using TapeStation, and the identified bands matched the expected genome sizes of 3.5, 4.0, 4.5, 4.6, 4.7, 4.8, and 4.9 kb, but not 5.0 or 5.5 kb, confirming the results of agarose gel electrophoresis (Figure 2B). These results suggest that the AAV genome is defective when the genome size is 5.0 kb or larger. Then, the AAV genome was analyzed using the nanopore long-read sequencing, and the nanopore sequencing read alignments were displayed in Integrative Genomics Viewer (IGV) (Figure 2C). The results of each nanopore sequencing run are also shown in Table S1. Consistent with the agarose gel electrophoresis and TapeStation results, the proportion of full-length genomes declined rapidly between 4.9 and 5.0 kb, with a more prominent decline occurring at 5.5 kb (Figure 2C and Table S1). The proportion of full-length genomes was significantly lower for the 5.0 kb genome (3.43 (2.40) %) than that for the 4.7 kb genome (24.97 (7.71) %) ($N = 3$ each, $p = 0.01$; Figure 2D). The proportion of full-length genomes decreased by 86.3% for the 5.0 kb genome compared with that for the 4.7 kb genome. Interestingly, both agarose gel electrophoresis and TapeStation indicated the near absence of full-length genome for the AAV 5.0 and 5.5 kb genomes, but a clear difference between the two was observed using the long-read sequencing, which indicated a progressive decrease in the proportion of full-length genomes even after 5.0 kb.

Furthermore, we investigated the AAV producer line to better understand the cause of the decreased proportion of full-length

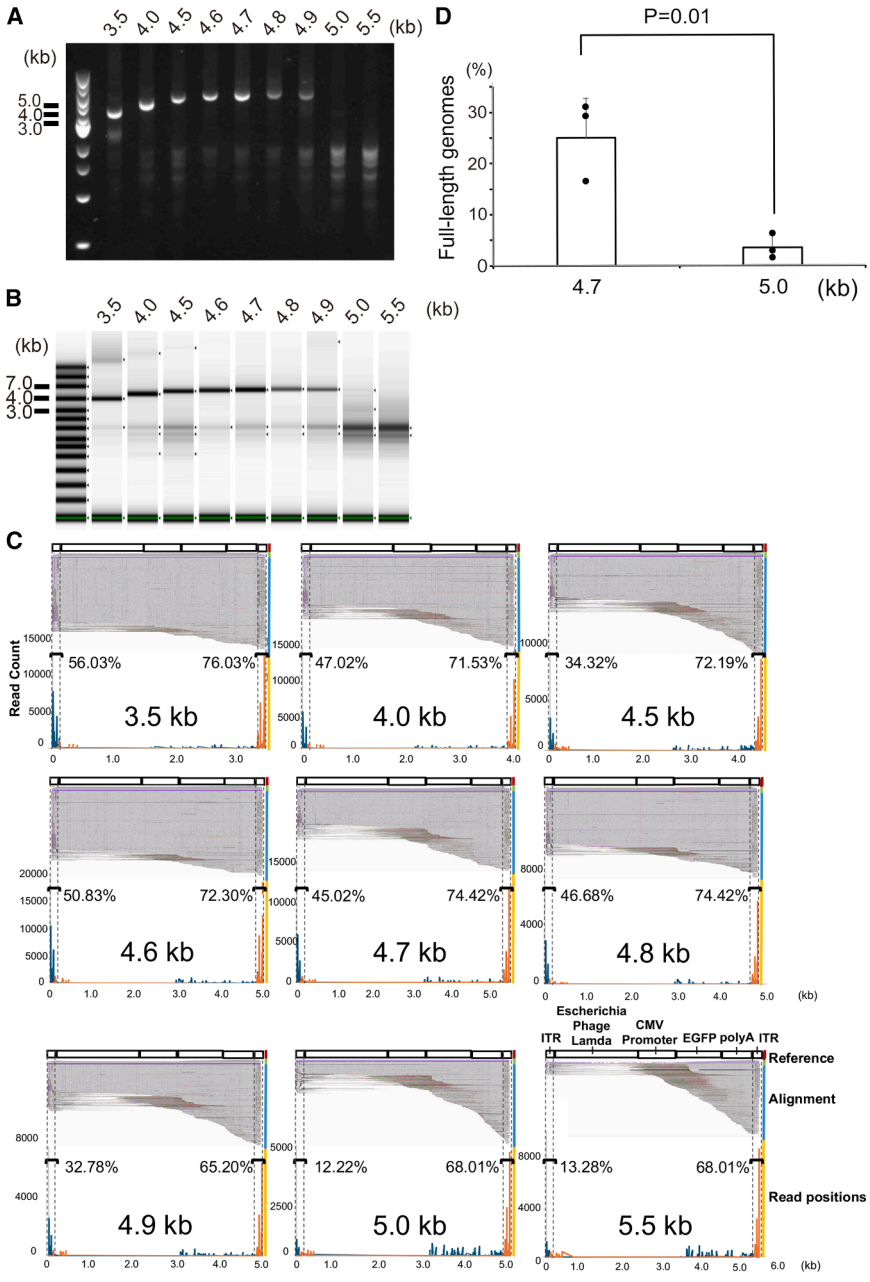

Figure 2. Rapid decline in the proportion of full-length AAV genomes between 4.9 and 5.0 kb

AAV vectors with various genome sizes were evaluated using (A) agarose gel electrophoresis, (B) TapeStation, and (C) nanopore sequencing. All evaluations showed a rapid decline in the proportion of full-length genomes between 4.9 and 5.0 kb. (D) The 4.7 kb had a significantly higher proportion of full-length genomes than the 5.0 kb using nanopore sequencing (N = 3 each, p = 0.01). Data are represented as mean (standard deviation). The p value was calculated using a t test (two-sided).

genomes in the oversized genome. We transfected HEK293T cells with AAV plasmids of 3.5 and 5.5 kb with and without the AAV capsid (*cap*) gene. We then compared the unpackaged (*cap* [−]) and packaged (*cap* [+]) genomes. Gel electrophoresis illustrated that the 5.5 kb genome was clearly visible in *cap* (−) samples but not in *cap* (+) samples without DNase treatment. The 3.5 kb genome was visible in both sample types (Figure 3). These results suggest that the full-length AAV genome is lost during the packaging process rather than during genome synthesis *per se*.

Identifying the pattern of functional genome components for each AAV vector using nanopore sequencing

Nanopore sequencing was used to examine the patterns of four functional genome components, namely, lambda phage spacer, cytomegalovirus (CMV) promoter, *EGFP*, and polyA, to determine the effects of the oversized AAV genome in more detail (Figures 4A and 4B). The pattern was similar for genome lengths of 3.5–4.8 kb, with many reads containing all four components, indicating the production of full-length genomes. However, small but significant changes were observed for 4.9 kb genomes, and 5.0 and 5.5 kb genomes exhibited drastically different patterns. A decrease in the proportion of full-length genomes, including all four components, was coupled with the generation of genomes containing EGFP and polyA at the 3′ end (Figure 4B). Of note, the full reporter expression cassette comprising the promoter, EGFP, and polyA was minimally included in AAV vectors with a genome size of at least 5.0 kb, and the promoter was missing in many of these genomes. Similarly, for an AAV vector of approximately 7.0 kb carrying *retinitis pigmentosa 1* (*RP1*), extremely few full-length reporter expression cassettes comprising the promoter, *RP1*, and polyA were included (Figure S1A). Gene region coverage was calculated by enumerating the number of reads at each genomic position (Figure S2). In these AAV vectors, coverage decreased significantly at the 5′ end for genome lengths of 4.9 kb and above.

Nanopore sequencing is known for its relatively high error rates.[22] When the read length and the error rate were compared, pAAV reads >1,000 bp exhibited uniform error rates and the shorter reads exhibited higher error rates. With regard to AAV, it was difficult to accurately evaluate the error rate by read length compared to pAAV since there was variation in the amount of packaged genomes

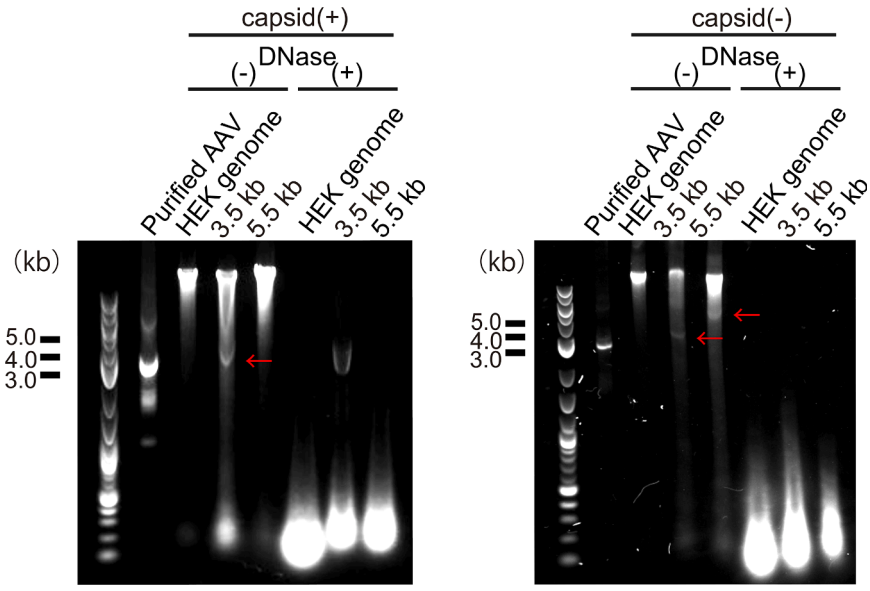

Figure 3. Agarose gel electrophoresis before and after DNase treatment with and without capsid gene

Without DNase treatment, the 5.5 kb genome was clearly visible in *cap* (–) samples but not in *cap* (+) samples, whereas the 3.5 kb genome was visible in both *cap* (–) and *cap* (+) samples. With DNase treatment, only the 3.5 kb genome with *cap* (+) was detected.

of different lengths (Figure S3). Furthermore, when the error rate for each genomic component was separately analyzed, the overall pattern remained relatively consistent across AAVs of different sizes, with a slightly higher error rate in the CMV promoter than in other components (Figure S4).

Reporter gene expression in the mouse retina for AAV vectors of different sizes

The expression of the EGFP reporter was evaluated in the retinas of mice injected subretinally with AAV vectors of different sizes (3.5, 4.0, 4.5, 5.0, and 5.5 kb). Histological analysis unexpectedly revealed robust EGFP expression in the photoreceptors for all vectors tested. Histological analysis of the retina revealed that reporter expression was similar for 3.5, 4.0, 4.5, and 5.0 kb vectors, but it was slightly reduced in the 5.5 kb vector (Figure 5A). The expression levels of EGFP for the 4.7, 5.0, and 5.5 kb vectors were confirmed using western blotting (Figures 5B and 5C). Consistent with the retinal histology results, the intensities of the 4.7 and 5.0 kb bands were similar but stronger than the intensity of the 5.5 kb band (Figure 5C). This is intriguing considering that the full reporter expression cassette consisting of the promoter, *EGFP*, and polyA sequences was barely packaged together in 5.0 and 5.5 kb vectors. These results indicate that the expression of the reporter gene located at the 3′ end does not necessarily parallel the proportion of full-length AAV genome packaging. We also tested AAV with an even larger genome of approximately 7.0 kb harboring *RP1* cDNA, a relatively frequent cause of retinitis pigmentosa.[23–26] This AAV vector exhibited a full-length genome proportion of 0.04% (Figure S1B), but it did not express *RP1*.

In vivo expression of Venus and mKO1 using AAV8.*CAG.Venus-GRK1-702.mKO1*

Expression of a reporter gene in the mouse retina was observed even with AAV vectors that had substantially reduced full-length packaging. This phenomenon might be partially explained by preferential packaging at the 3′ end, where *EGFP* and its polyA are located. However, the normal expression of the reporter gene in the near absence of the driving promoter is perplexing. Furthermore, it remains unclear whether the observed pattern, i.e., preferential packaging of components at the 3′ end, is common to vectors with oversized genomes or it varies among different designs of oversized vectors. To address this issue, we inserted the Venus reporter gene, which is 98.1% homologous with *EGFP* at the 5′ end, and placed another reporter gene, such as *mKO1*, with 26.0% homology with *EGFP* at the 3′ end, in a head-to-head configuration. The resulting AAV vector with a 5.3 kb genome containing each reporter gene encoded a fluorescent protein of a different spectrum (AAV8.*CAG.Venus-GRK1-702.mKO1*). Then, the AAV genome was analyzed using the nanopore long-read sequencing (Figure 6A). The proportion of the packaged full-length genomes was 0.19% for AAV8.*CAG.Venus-GRK1-702.mKO1*. Interestingly, relocating *Venus* to the 5′ end resulted in preferential packaging of both the 5′ and 3′ ends, indicating that the effect of the large AAV genome on packaging differed substantially between vectors of different designs. Analysis of the functional components of the genome revealed that the polyA ends of the genome were preferentially packaged, sometimes together with the neighboring reporter gene but most commonly without the promoter (Figure 6B). AAV8.*CAG.Venus-GRK1-702.mKO1* was injected subretinally in the mouse eye, and the expression of Venus and mKO1 was verified with western blotting (Figure 6C) and histological analysis (Figure 6D). This result also implies that protein expression requires a small number of incomplete functional copies, even with a minimal amount of the promoter sequence driving expression.

DISCUSSION

In this study, the nanopore long-read sequencing was effectively used to assess the genome integrity of AAV vectors, offering important insights that are not achievable with conventional short-read sequencing or gel electrophoresis-based methods. The AAV vectors included an EGFP expression cassette along with lamba phage spacer sequences of varying sizes, enabling the production of a wide range of AAV genomes of different sizes. This approach allowed us to better define the capacity of AAV cargo, which has remained unclear to date.[4–6] The proportion of packaged full-length AAV genomes of 5.0

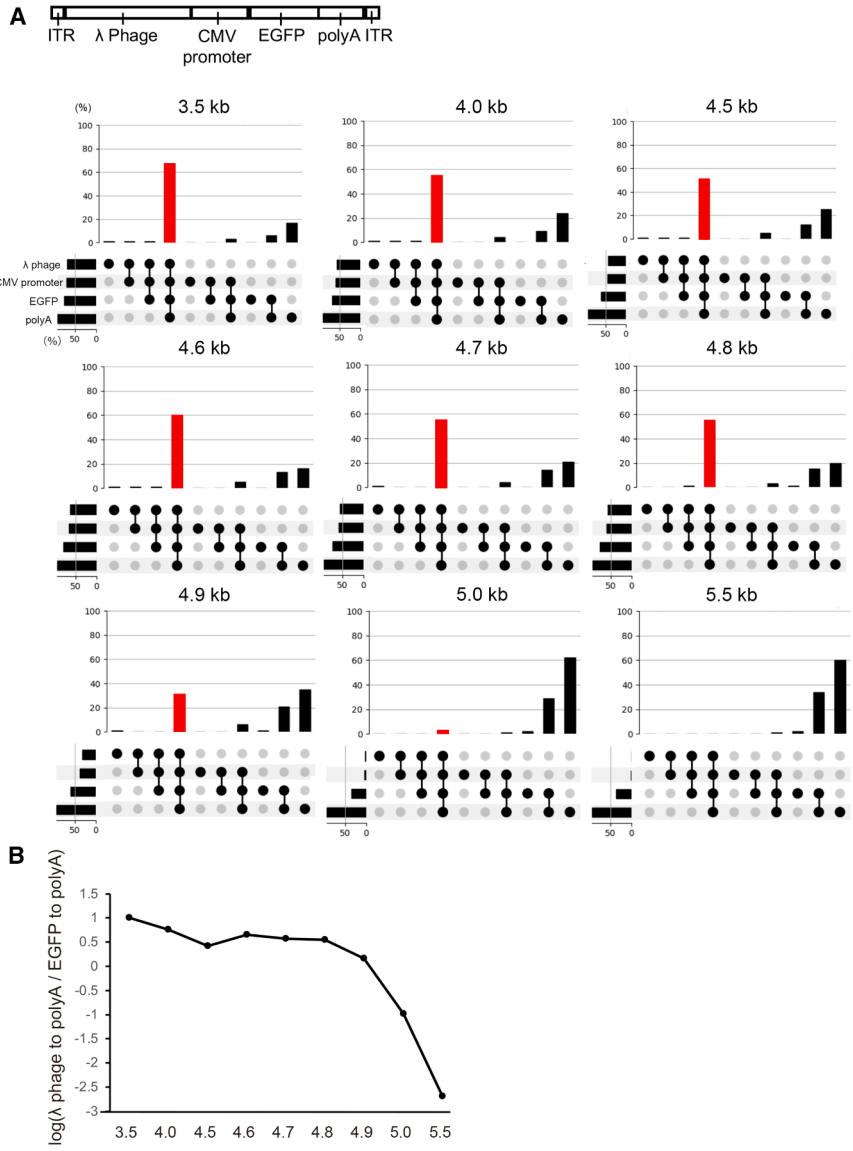

Figure 4. Decreased proportion of full-length AAV genomes coupled with an increased proportion of short genomes retaining only EGFP and polyA at the 3′ end

Nanopore sequencing analysis of the AAV genome with functional components. A schematic representation of the AAV vector constructs is shown at the top of the figure. (A) Analysis of the 10 major patterns of the packaged genome in AAVs of different sizes. The black circles indicate the fully mapped components. The bar graph above the map indicates the percentage of reads within each AAV vector. The bar graph in the lower left displays the percentage of reads for each genomic component. The pattern was similar for AAV genomes from 3.5 to 4.8 kb in length, but small changes were observed in AAV genomes from 4.9 kb and larger. The 5.0 and 5.5 kb genomes show a completely different pattern. (B) Changes in the patterns of the packaged genome for AAV vectors of different sizes. The ratio between the percentages of full reads from lamba phage to polyA and the percentage of reads from *EGFP* to polyA was calculated and plotted on a logarithmic graph. A change was observed in genomes above 4.9 kb, with the 5.0 and 5.5 kb showing markedly different patterns.

kb or larger was greatly reduced, which was attributable to the defect in the packaging of the genome rather than its synthesis. More importantly, analysis using the nanopore system showed that the pattern of the packaged AAV genome was modestly but clearly altered at 4.9 kb, a difference that could not be detected with conventional DNA analysis. Thus, the upper limit for efficient gene delivery of AAV vectors lies around 4.9 kb, and the full-length genome rapidly deteriorates when the genome size surpasses this threshold, as observed in our study. This information is critically important when designing AAV vectors for clinical gene therapy, which often has a very narrow titer window between effectiveness and toxicity.[27,28] This narrow titer window hampers the production of effective AAV products with minimal inflammation and local tissue damage.[29,30] Our study also revealed short genomic fragments with incomplete packaging, which were difficult to detect in previous studies. For effective gene transfer using AAV, the abundance ratios of AAV packaged with short fragments should be minimized. The results of this study also highlight the strength of using long-read sequencing to assess the genomic integrity of the AAV vectors.

Our results using the long-read sequencing provide detailed insights into the defective packaging of the oversized AAV genome. Our study demonstrated that oversized AAV genomes are mainly packaged with shorter fragments and the loss of the full-length genomes in oversized AAV vectors was coupled with the inclusion of an incomplete AAV genome retaining a small 3′ end genomic fragment. Previous studies suggest that even oversized AAV genomes can be packaged to the limit of packaging and small genome fragments are preferentially packaged by Southern blot.[4,31] However, when a close homolog of *EGFP* was placed at the 5′ end, an incomplete AAV genome containing the 5′ end was also detected. These results indicate that the patterns of packaged genome differ between vectors with varying designs and highlight the importance of analyzing each AAV vector with long-read sequencing, particularly for clinical applications. Of note, a significant reduction in the packaging of a reporter expression cassette did not always result in the equivalent loss of reporter protein expression. For example, compared with the 4.7 kb construct, the 5.0 kb construct exhibited 91.5% deficiency in the reporter expression cassette and 52.0% deficiency in the reporter gene itself;

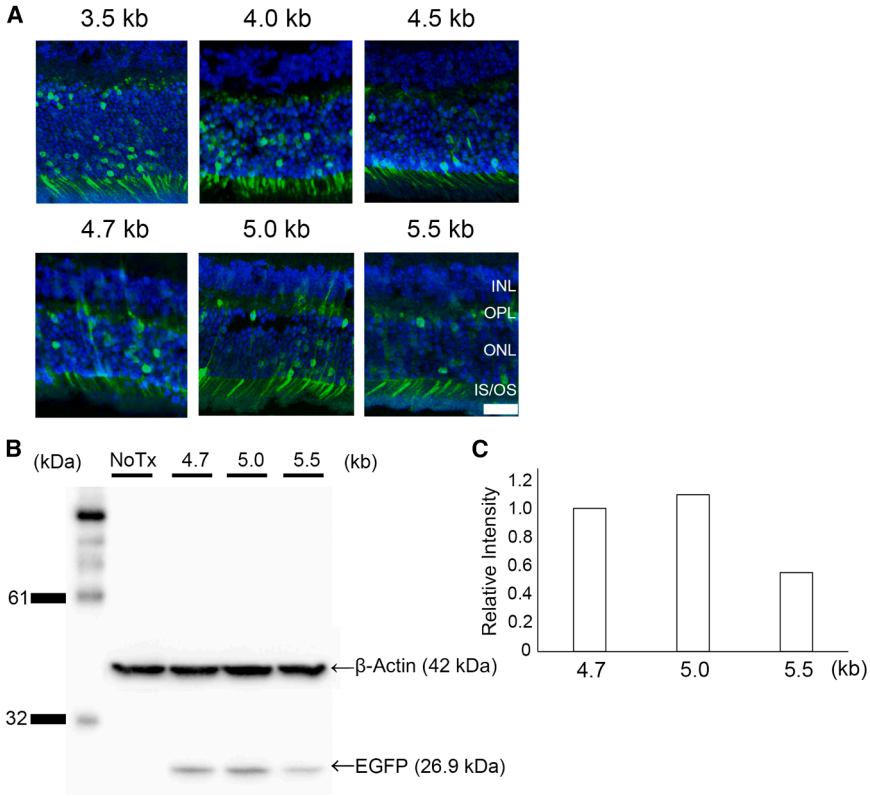

Figure 5. Reporter EGFP expression in mice using oversized AAV vectors with low proportions of full-length genomes

EGFP expression was assessed in mouse retinas after subretinal injections with AAV vectors of various sizes. (A) A significant number of EGFP-positive photoreceptors were observed after the injection of AAV8-*EGFP* vectors with genome sizes ranging from 3.5 to 5.5 kb. A rapid decline in reporter protein expression was not detected between 4.7 and 5.0 kb genomes. Scale bars: 20 μm. (B) Western blotting of EGFP after injection of AAVs with genome sizes of 4.7, 5.0, and 5.5 kb. (C) Quantification of the western blotting revealed unchanged EGFP expression at 5.0 kb followed by a moderate decline at 5.5 kb relative to 4.7 kb AAV vector genome sizes. INL, inner nuclear layer; OPL, outer plexiform layer; ONL, outer nuclear layer; IS/OS, inner segment/outer segment; NoTx, no treatment.

however, these deficiencies did not lead to significant changes in the expression of the protein. A plausible explanation is that full-length EGFP expression cassettes form inside transduced cells when the (+) strand genome pairs with the (−) strand genome from fragmented AAV vectors. DNA polymerase then repairs this structure, creating a full-length double-stranded DNA cassette. This could partly explain the gaps between AAV genome content and actual gene expression, a phenomenon also noted in previous studies.[4,32–35] In addition, mechanisms such as overlapping sequences and *trans*-splicing—in which two separate AAV vectors combine to restore gene expression—have been explored for treating diseases caused by large genes that exceed the packaging limit of AAV.[36–42] Although ITRs can potentially function as promoters,[43,44] their capacity to match or outperform the ubiquitous high-performance CMV promoter is unclear, especially if the reads containing the reporter gene material were substantially reduced. However, even considering these possibilities, the starting material for the *EGFP* gene is extremely limited because of defective genome packaging in large AAV vectors. This raises uncertainty about whether these processes fully explain the observed gap.

Moreover, the proportion of the packaged full-length AAV8.*GRK1-93.RP1* vector was as low as 0.04% (Figure S1) for the 7 kb AAV vector carrying *RP1* cDNA. *RP1* is a causative gene for retinitis pigmentosa, which is difficult to treat with gene therapy due to its large gene size. However, at least 0.04% of full-length reads were detected, suggesting that AAV vectors can facilitate the introduction of large genes with a highly accurate purification method in the future.

This study had several limitations. First, the DNA packaging of oversized genomes may depend on the design of the vector, and we have only examined specific designs. In addition, we did not evaluate serotypes other than AAV8; thus, the applicability of the results to other AAV serotypes is unclear. A larger number of vectors of different designs should be analyzed with long-read sequencing to resolve these issues. Second, we could not assess the possible mechanisms of retained reporter expression when its genomic counterpart and promoter were poorly detected, which includes the intracellular reconstitution of the reporter gene, to fill the gap observed in the oversized AAV vectors. Similarly, we excluded ITR sequences from our evaluation because a full-length ITR is difficult to read with the sequencing, possibly due to adapter binding to the secondary structure of the ITR.[15] Therefore, we did not explore the possibility of the ITR functioning as a promoter. Lastly, the *in vivo* study was only conducted in mice. Exploring the discrepancy between AAV genome integrity and transgene expression in more clinically relevant animal models, such as primates, is essential.

In conclusion, the current study highlights the utility of long-read sequencing in assessing the genomic integrity of AAV vectors. This is particularly important in designing AAV vectors that surpass 4.7 kb, as the arrangement of genomic components may affect the pattern of packaged DNA.

MATERIALS AND METHODS

Animals

C57BL/6J mice (6 weeks old; Japan SLC Inc., Hamamatsu, Japan) were used for the retina studies.[8,45] The mice were maintained under

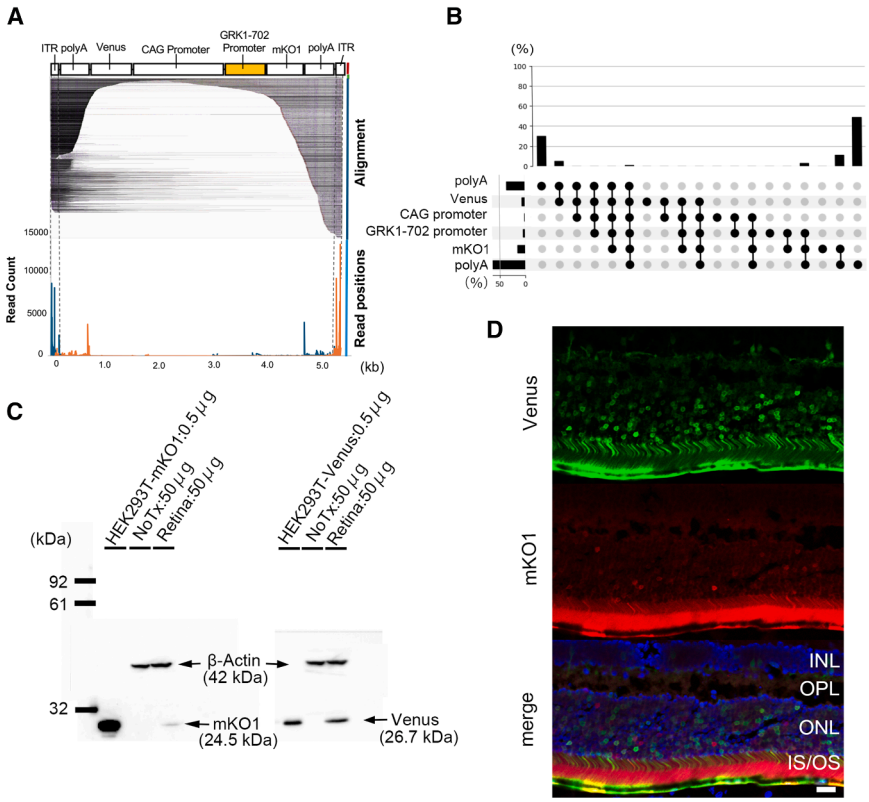

Figure 6. Retained reporter gene and expression at the 3′ end in AAV with an oversized genome

(A) An oversized AAV vector (5.3 kb) with *Venus* at the 5′ end and *mKO1* at the 3′ end (AAV8.*CAG.Venus-GRK1-702.mKO1*) was analyzed using nanopore sequencing. The packaged genome was observed at both the 5′ and 3′ ends. (B) Analysis of the patterns of the packaged genome by functional genomic components in AAV8.*CAG.Venus-GRK1-702.mKO1*. (C) The western blotting of murine retinas injected with AAV.*CAG.Venus-GRK1-702.mKO1*. Marked Venus and mKO1 expression was confirmed. (D) Representative retinal histology showing Venus and mKO1 expression in the photoreceptors of mice treated with the AAV vector. Scale bars: 20 μm. INL, inner nuclear layer; OPL, outer plexiform layer; ONL, outer nuclear layer; IS/OS, inner segment/outer segment; mKO1, monomeric Kusabira-Orange 1; NoTx, no treatment.

a 12-h light and 12-h dark cycle and allowed free access to food and water. Surgical procedures were conducted under deep anesthesia using intraperitoneal ketamine (37.5 mg/kg) and medetomidine (0.625 mg/kg). The effects of medetomidine were reversed with an intraperitoneal injection of atipamezole (0.25 mg/kg). All animal experiments complied with the guidelines of the Association for Research in Vision and Ophthalmology for the Use of Animals in Ophthalmic and Vision Research. All experimental procedures were approved by the Ethics Committee for Animal Experiments at Nagoya University Graduate School of Medicine.

Purified AAVs of different sizes were injected into both eyes of the mice. Each vector (1.0×10^{12} genome copies/mL; 2.0 μL per injection) was injected subretinally. Four weeks after injection, the eyes were enucleated and processed for histological evaluation and western blotting.

Construction and purification of plasmids and AAV vectors

The assembly of AAV vectors is shown in Figure 1A. The primers are shown in Table S2. pAAV-*CMV*::*EGFP* was constructed by subcloning the CMV promoter and EGFP from pEGFP-N1 (Clontech Laboratories, Inc., Mountain View, CA) into pAAV-MCS (Cell Biolabs Inc., San Diego, CA). The λDNA fragments were amplified to the final AAV genome sizes of 3.5, 4.0, 4.5, 5.0, and 5.5 kb with KOD One PCR Master Mix (Toyobo Co., Ltd., Osaka, Japan) using λDNA (Takara Bio Inc., Shiga, Japan) as a template. The amplified λDNA fragments were digested with *Eco*RI and *Sal*I-HF (New England Biolabs, Inc, Ipswich, MA) and inserted into pAAV-*CMV*::*EGFP* using a DNA Ligation Kit (Takara Bio Inc.). For the 4.6, 4.7, and 4.9 kb constructs, the λDNA fragments were amplified as described previously and inserted into the pAAV-λDNA *CMV*::*EGFP* vector (4.5 kb) at the *Hind*III-HF and *Sal*I-HF (New England Biolabs, Inc) sites. For the 4.8 kb construct, a λDNA fragment was inserted into pAAV-λDNA *CMV*::*EGFP* (4.7 kb) using the NEBuilder HiFi DNA Assembly Kit (New England Biolabs, Inc). To construct AAV8.*CAG*::*Venus-GRK1-702*::*mKO1,* the *GRK1-702* fragment was amplified using KOD One PCR Master Mix (Toyobo Co., Ltd.) and a human genome template; the *mKO1* cDNA (Medical & Biological Laboratories Co., Ltd., Nagoya, Japan) was inserted into pAAV-MCS (Cell Biolabs Inc.), followed by the CAG promoter (from pCAG-NEO; FUJIFILM Wako Pure Chemical Corp., Osaka, Japan) and *Venus*[46] (synthesized by Eurofins Genomics, Tokyo, Japan) in the reverse direction to *GRK1-702*::*mKO1* using the NEBuilder HiFi DNA Assembly Kit (New England Biolabs, Inc). The *GRK1-93* promoter was used to construct the *RP1*-expressing AAV vector.[8] This promoter was expressed well in cultured monkey and mouse retinas (Figure S5). The *GRK1-93* oligonucleotide fragment was subcloned into pAAV-MCS (Cell Biolabs Inc.) using a DNA Ligation Kit (Takara Bio Inc.). For AAV8.*GRK1-93.RP1,* the *RP1* fragment with a tag (HA-tag, FLAG tag, and Strep-tag) was amplified using KOD One PCR Master Mix (Toyobo Co., Ltd.) with the *RP1* open reading frame clone (ORS12477; Promega, Madison, WI; GenBank: NM_006269.2) and inserted into the vector using the NEBuilder HiFi DNA Assembly Kit (New England Biolabs, Inc). To construct AAV-*cap* (−), the capsid gene was removed from pAAV-RC2 (Cell Biolabs Inc.) via digestion by the restriction enzyme *Bst*BI (New England Biolabs, Inc) and then self-ligated using a DNA Ligation Kit (Takara Bio Inc.). The ligation samples were transformed using DH5a-competent cells (Toyobo Co., Ltd.). Plasmids were extracted

using the Fast Gene Plasmid Mini Kit (NIPPON Genetics Co., Ltd., Tokyo, Japan).

The extracted plasmids were subjected to Sanger sequencing to confirm donor insertion. Plasmids were further extracted using Nucleobond Xtra Midi EF (Takara Bio Inc.). The constructed plasmid vectors were assembled into AAV2/8 as previously described.[8] Each vector was co-transfected with the AAV2*rep*/AAV8*cap* vector (pdp8; PlasmidFactory GmbH & Co. KG, Bielefeld, Germany) in HEK293T cells. AAV8.*GRK1-93.RP1* was generated using AAV-Max (Thermo Fisher Scientific, Waltham, MA), following the manufacturer's instructions. AAV particles were extracted with PBS and purified using an AKTA go chromatography system (Cytiva, Chicago, IL) on a HiTrap AVB Sepharose HP column (Cytiva, Chicago, IL).[45,47] Endotoxin was tested using Limulus Amebocyte Lysate PYROGENT-5000 (Lonza Group AG, Walkersville, MD); all vectors had lipopolysaccharide (LPS) levels <1.25 endotoxin units (EU)/mL. DNA was extracted from AAVs using phenol–chloroform. The AAV genome was detected using agarose gel electrophoresis and the ChemiDoc XRS+ System (Bio-Rad Laboratories, Inc., Hercules, CA).

The AAV genome size was estimated by quantifying genomic DNA with the Agilent 4150 TapeStation system (Agilent Technologies, Inc., Santa Clara, CA), Genomic DNA Reagent (Agilent Technologies, Inc.), and Genomic DNA ScreenTape (Agilent Technologies, Inc.). For the analysis of *cap* (−) and *cap* (+) genomes, the lysates were treated with proteinase K and subjected to DNA extraction using a DNA extraction kit (QIAamp DNA Mini kit; QIAGEN, Hilden, Germany). For samples treated with benzonase (2 μL per 1 mL of sample), benzonase was removed via phenol-chloroform extraction, followed by DNA extraction.

Nanopore sequencing

After digesting plasmids with *Sbf*I-HF (New England Biolabs, Inc.), the DNA was extracted and purified from AAVs using phenol-chloroform. Libraries for nanopore sequencing were prepared according to the manufacturer's instructions for ligation sequencing of gDNA (SQK-LSK110; Oxford Nanopore Technologies plc, Oxford, UK). The NEB Next companion module (New England Biolabs, Inc.) and Ligation Sequencing Kit (SQK-LSK110; Oxford Nanopore Technologies plc) were used for DNA preparation and adaptor ligation. DNA was quantified with a Qubit 4.0 fluorometer (Thermo Fisher Scientific). DNA samples were cleaned with AMPure XP beads. Fragment sizes and molar concentrations of each library were determined with the Agilent 4150 TapeStation system, Genomic DNA ScreenTape, and Genomic DNA Reagent (Agilent Technologies, Inc.). Libraries were adjusted using Flongle Sequencing Expansion (EXP-FSE001; Oxford Nanopore Technologies plc) and loaded into the Flongle Flow Cell (FLO-FLG001, R9.4.1; Oxford Nanopore Technologies plc), which was set up in MinION (Oxford Nanopore Technologies plc) with a run time of 24 h.

The genome was visualized using nanopore sequencing as previously described.[9] MinKNOW (v5.8.12) was used for basecalling. Minimap2 was used to align the sequencing reads with the appropriate reference sequences,[48,49] and the alignments were visualized in IGV (v2.12.2)[50–53] with soft clipping. The start and end positions of the aligned reads, the proportions of full-length genomes, and the full mapping percentage for each gene were calculated using browser extensible data (BED) files. The reads mapping completely to the reference sequence of each gene inside the ITRs were defined as full-length reads, and the proportions of full-length genomes of the AAV constructs were calculated. Coverage of the packaged vector was calculated and visualized by counting the number of nucleotides mapped to each position of the reference sequence using BED files. All aforementioned calculations were performed with Python (version 3.12.3). The percentages of reads mapped to plasmid/vector were calculated using the bam files.

To calculate the error rates, we divided the number of mismatches and indels in each read mapped to the sequence between the ITR by the reference alignment length using bam files. We displayed the error rate distribution for each alignment length as a hexbin plot. The error rates for each genome component were calculated in a similar manner using the same bam files. All calculations were performed using Python (version 3.12.8), and figures were drawn in R (version 4.3.3).

Western blotting

Western blotting was performed as previously described.[8,47,54] The retinas and retinal pigment epithelium (RPE)/choroid complexes were separated, and the retinas were cut into small pieces and dissolved in RIPA buffer (Merck KGaA, Darmstadt, Germany) at 4°C. Protein concentrations were determined using a Pierce BCA protein assay kit (Takara Bio Inc.). For the AAV 4.7, 5.5, and 5.5 kb constructs, mouse retinal proteins (25 μg each) were separated using SDS-PAGE with 5%–20% SuperSep Ace (FUJIFILM Wako Pure Chemical Corp.) and transferred to polyvinylidene fluoride membranes (Immobilion Transfer Membrane, 0.45 μm, Merck KGaA). For AAV8.*CAG::Venus-GRK1-702.mKO1*, mouse retinal proteins (50 μg) were separated and HEK293T lysates (0.5 μg) expressing Venus and mKO1 were used as positive controls. For AAV8.*GRK1-93.RP1*, mouse retinal proteins (100 μg) were separated and WERI Rb-1 cell lysates (5 μg) transfected with pAAV8.*GRK1-93.RP1* plasmid were used as a positive control. After blocking membranes with 5% skim milk in PBS-T (0.05 M Tris, 0.138 M NaCl, 0.0027 M KCl, pH 8.0, and 0.05% Tween 20; Sigma-Aldrich, St. Louis, MO) for 1 h, the membranes were incubated with rabbit anti-GFP antibody (#598, 1/1000; Medical & Biological Laboratories Co., Ltd.), anti-monomeric Kusabira-Orange 2 pAb (PM051M, 1/500; Medical & Biological Laboratories Co., Ltd.), monoclonal anti-FLAG M2, Clone M2 (F1804, 1/2000; Merck KGaA), and monoclonal anti-β-actin mouse (A5316, 1/5000; Merck KGaA) at 4°C overnight. The membranes were then incubated for 1 h with horseradish peroxidase (HRP)-conjugated anti-rabbit IgG antibody (A0545, 1/5000; Merck KGaA) or HRP-conjugated Goat anti-Mouse IgG (H + L) antibody (#31430, 1/5000; Thermo Fisher Scientific). The immunogenic signal was visualized with ECL Prime Western

Blotting Detection Reagent (Cytiva) and the ChemiDoc XRS+ System. The protein band intensities were quantified using ImageJ software (National Institutes of Health, Bethesda, MD), and differences were assessed by calculating the relative intensity normalized to the intensity of AAV8-4.7 kb.

Histology

Enucleated eyes were fixed in 4% paraformaldehyde, embedded in OCT compound (Tissue-Tek OCT; Sakura Finetek USA, Inc., Torrance, CA), and sectioned (10 μm thick) using a cryostat (CM3050 S; Leica Microsystems GmbH, Wetzlar, Germany). Retinal sections expressing EGFP, Venus, and mKO1 were covered with VECTASHIELD Antifade Mounting Medium with DAPI (Vector Laboratories, Inc., Burlingame, CA). Images were acquired using Zeiss LSM880-ELYRA PS. 1 (Carl Zeiss AG, Jena, Germany).

Monkey retinal explant culture

Monkey retinal explant culture was performed as previously described.[55] Monkey eyes were obtained immediately after sacrifice at the Primate Research Institute of Kyoto University and incubated within 5 h after enucleation. The neural retina was isolated, and 3-mm biopsy punches were obtained from the neural retina of both eyes. Retinal punches were transferred to nucleopore membranes of Millicell cell culture inserts (0.4 μm, 30 mm diameter; Merck KGaA) with the outer retina (photoreceptor side) facing down. The inserts were placed in 6-well tissue culture plates (AS ONE Corp. Osaka, Japan) containing enough medium (Neurobasal-A medium [Thermo Fisher Scientific] + N2 Supplement [Thermo Fisher Scientific] + B27 Plus Supplement [Thermo Fisher Scientific] + L-Glutamine Solution [FUJIFILM Wako Pure Chemical Corp.] + 1% penicillin/streptomycin [Thermo Fisher Scientific]) to moisten the membrane. Vectors (10 μL at 1×10^{12} genome copies/mL) were injected between the neural retina and nucleopore membrane using an ITO microsyringe (ITO Corp., Shizuoka, Japan) with compatible needles (ITO Corp.) to form a viral bleb under the retina. After incubating retinal tissues at 37°C and 5% CO_2 for 1 h, 900 μL of medium per well was added under the nucleopore membrane, and 25 μL was carefully added to each retina. Retinal tissues were incubated while replacing the medium every 2 days. After 28 days, the tissues were collected and processed for histological evaluation.

Statistical analysis

Statistical analyses were performed using the IBM SPSS software package (v29.0, IBM Corp., Armonk, NY) or R (version 4.3.3). Differences between two groups were assessed using unpaired Student's t tests. All values are expressed as means with standard deviations (N = number of samples). $p < 0.05$ was considered statistically significant.

DATA AVAILABILITY

All data directly relevant to the study are included in the manuscript or supplementary materials. For further inquiries, please contact the corresponding author.

ACKNOWLEDGMENTS

The study was supported in part by JSPS KAKENHI grants (21K09673 and 24K12781 to K.F. and 23K27750 to K.M.N.) from the Japan Agency for Medical Research and Development (23ek0109660h0001 to K.M.N.). We thank the Division for Medical Research Engineering of Nagoya University Graduate School of Medicine for technical support.

AUTHOR CONTRIBUTIONS

K.M.N. conceived and designed the experiments. M.K. and K.F. designed and constructed the vectors. M.K. and A.F.S. acquired and analyzed the data. M.K. and K. Yamada performed the *in vivo* experiments. K.H. and T.M. were involved in the experimental execution. M.T., N.S., and K.-i.I. contributed to the monkey studies. M.K. drafted the original manuscript. A.F.S., K.F., K. Yamada, K. Yuki, and K.M.N. revised and edited the manuscript. The final manuscript was read and approved by all authors.

DECLARATION OF INTERESTS

K.M.N. received funding from JCR Pharma, Ltd, and K.M.N. and K.F. hold a patent related to the promoter sequence used in the study.

DECLARATION OF GENERATIVE AI AND AI-ASSISTED TECHNOLOGIES IN THE WRITING PROCESS

During the preparation of this work, the authors used DeepL, ChatGPT, and Grammarly in order to improve readability and language. After using these tools, the authors reviewed and edited the content as needed and take full responsibility for the content of the publication.

SUPPLEMENTAL INFORMATION

Supplemental information can be found online at https://doi.org/10.1016/j.omtm.2025.101474.

REFERENCES

1. Kumaran, N., Michaelides, M., Smith, A.J., Ali, R.R., and Bainbridge, J.W.B. (2018). Retinal gene therapy. Br. Med. Bull. *126*, 13–25. https://doi.org/10.1093/bmb/ldy005.
2. Liu, X., Qiao, J., Jia, R., Zhang, F., Meng, X., Li, Y., and Yang, L. (2023). Allele-specific gene-editing approach for vision loss restoration in RHO-associated retinitis pigmentosa. Elife *12*, e84065. https://doi.org/10.7554/eLife.84065.
3. Sakai, D., Hiraoka, M., Matsuzaki, M., Yokota, S., Hirami, Y., Onishi, A., Nakamura, M., Takahashi, M., Kurimoto, Y., and Maeda, A. (2023). Genotype and phenotype characteristics of RHO-associated retinitis pigmentosa in the Japanese population. Jpn. J. Ophthalmol. *67*, 138–148. https://doi.org/10.1007/s10384-023-00975-y.
4. Wu, Z., Yang, H., and Colosi, P. (2010). Effect of genome size on AAV vector packaging. Mol. Ther. *18*, 80–86. https://doi.org/10.1038/mt.2009.255.
5. Ibreljic, N., Draper, B.E., and Lawton, C.W. (2024). Recombinant AAV genome size effect on viral vector production, purification, and thermostability. Mol. Ther. Methods Clin. Dev. *32*, 101188. https://doi.org/10.1016/j.omtm.2024.101188.
6. Dong, J.Y., Fan, P.D., and Frizzell, R.A. (1996). Quantitative analysis of the packaging capacity of recombinant adeno-associated virus. Hum. Gene Ther. *7*, 2101–2112. https://doi.org/10.1089/hum.1996.7.17-2101.
7. Naso, M.F., Tomkowicz, B., Perry, W.L., 3rd, and Strohl, W.R. (2017). Adeno-associated virus (AAV) as a vector for gene therapy. BioDrugs *31*, 317–334. https://doi.org/10.1007/s40259-017-0234-5.
8. Nishiguchi, K.M., Fujita, K., Miya, F., Katayama, S., and Nakazawa, T. (2020). Single AAV-mediated mutation replacement genome editing in limited number of photoreceptors restores vision in mice. Nat. Commun. *11*, 482. https://doi.org/10.1038/s41467-019-14181-3.
9. Ibraheim, R., Tai, P.W.L., Mir, A., Javeed, N., Wang, J., Rodríguez, T.C., Namkung, S., Nelson, S., Khokhar, E.S., Mintzer, E., et al. (2021). Self-inactivating, all-in-one AAV vectors for precision Cas9 genome editing via homology-directed repair in vivo. Nat. Commun. *12*, 6267. https://doi.org/10.1038/s41467-021-26518-y.
10. Adachi, K., Enoki, T., Kawano, Y., Veraz, M., and Nakai, H. (2014). Drawing a high-resolution functional map of adeno-associated virus capsid by massively parallel sequencing. Nat. Commun. *5*, 3075. https://doi.org/10.1038/ncomms4075.

11. Saveliev, A., Liu, J., Li, M., Hirata, L., Latshaw, C., Zhang, J., and Wilson, J.M. (2018). Accurate and rapid sequence analysis of adeno-associated virus plasmids by Illumina next-generation sequencing. Hum. Gene Ther. Methods *29*, 201–211. https://doi.org/10.1089/hgtb.2018.037.

12. de Koning, W., Miladi, M., Hiltemann, S., Heikema, A., Hays, J.P., Flemming, S., van den Beek, M., Mustafa, D.A., Backofen, R., Grüning, B., and Stubbs, A.P. (2020). NanoGalaxy: Nanopore long-read sequencing data analysis in Galaxy. GigaScience *9*, giaa105. https://doi.org/10.1093/gigascience/giaa105.

13. Deamer, D., Akeson, M., and Branton, D. (2016). Three decades of nanopore sequencing. Nat. Biotechnol. *34*, 518–524. https://doi.org/10.1038/nbt.3423.

14. Jain, M., Olsen, H.E., Paten, B., and Akeson, M. (2016). The Oxford Nanopore MinION: delivery of nanopore sequencing to the genomics community. Genome Biol. *17*, 239. https://doi.org/10.1186/s13059-016-1103-0.

15. Namkung, S., Tran, N.T., Manokaran, S., He, R., Su, Q., Xie, J., Gao, G., and Tai, P. W.L. (2022). Direct ITR-to-ITR nanopore sequencing of AAV vector genomes. Hum. Gene Ther. *33*, 1187–1196. https://doi.org/10.1089/hum.2022.143.

16. Chapman, R., Jones, L., D'Angelo, A., Suliman, A., Anwar, M., and Bagby, S. (2023). Nanopore-based metagenomic sequencing in respiratory tract infection: A developing diagnostic platform. Lung *201*, 171–179. https://doi.org/10.1007/s00408-023-00612-y.

17. Wang, Y., Zhao, Y., Bollas, A., Wang, Y., and Au, K.F. (2021). Nanopore sequencing technology, bioinformatics and applications. Nat. Biotechnol. *39*, 1348–1365. https://doi.org/10.1038/s41587-021-01108-x.

18. Schmidt, K., Mwaigwisya, S., Crossman, L.C., Doumith, M., Munroe, D., Pires, C., Khan, A.M., Woodford, N., Saunders, N.J., Wain, J., et al. (2017). Identification of bacterial pathogens and antimicrobial resistance directly from clinical urines by nanopore-based metagenomic sequencing. J. Antimicrob. Chemother. *72*, 104–114. https://doi.org/10.1093/jac/dkw397.

19. Charalampous, T., Kay, G.L., Richardson, H., Aydin, A., Baldan, R., Jeanes, C., Rae, D., Grundy, S., Turner, D.J., Wain, J., et al. (2019). Nanopore metagenomics enables rapid clinical diagnosis of bacterial lower respiratory infection. Nat. Biotechnol. *37*, 783–792. https://doi.org/10.1038/s41587-019-0156-5.

20. Brejová, B., Boršová, K., Hodorová, V., Čabanová, V., Gafurov, A., Fričová, D., Neboháčová, M., Vinař, T., Klempa, B., and Nosek, J. (2021). Nanopore sequencing of SARS-CoV-2: Comparison of short and long PCR-tiling amplicon protocols. PLoS One *16*, e0259277. https://doi.org/10.1371/journal.pone.0259277.

21. Chan, W.S., Au, C.H., Lam, H.Y., Wang, C.L.N., Ho, D.N.-Y., Lam, Y.M., Chu, D.K. W., Poon, L.L.M., Chan, T.L., Zee, J.S.-T., et al. (2020). Evaluation on the use of Nanopore sequencing for direct characterization of coronaviruses from respiratory specimens, and a study on emerging missense mutations in partial RdRP gene of SARS-CoV-2. Virol. J. *17*, 183. https://doi.org/10.1186/s12985-020-01454-3.

22. Jain, M., Koren, S., Miga, K.H., Quick, J., Rand, A.C., Sasani, T.A., Tyson, J.R., Beggs, A.D., Dilthey, A.T., Fiddes, I.T., et al. (2018). Nanopore sequencing and assembly of a human genome with ultra-long reads. Nat. Biotechnol. *36*, 338–345. https://doi.org/10.1038/nbt.4060.

23. Bowne, S.J., Daiger, S.P., Hims, M.M., Sohocki, M.M., Malone, K.A., McKie, A.B., Heckenlively, J.R., Birch, D.G., Inglehearn, C.F., Bhattacharya, S.S., et al. (1999). Mutations in the RP1 gene causing autosomal dominant retinitis pigmentosa. Hum. Mol. Genet. *8*, 2121–2128. https://doi.org/10.1093/hmg/8.11.2121.

24. Pierce, E.A., Quinn, T., Meehan, T., McGee, T.L., Berson, E.L., and Dryja, T.P. (1999). Mutations in a gene encoding a new oxygen-regulated photoreceptor protein cause dominant retinitis pigmentosa. Nat. Genet. *22*, 248–254. https://doi.org/10.1038/10305.

25. Payne, A., Vithana, E., Khaliq, S., Hameed, A., Deller, J., Abu-Safieh, L., Kermani, S., Leroy, B.P., Mehdi, S.Q., Moore, A.T., et al. (2000). RP1 protein truncating mutations predominate at the RP1 adRP locus. Investig. Ophthalmol. Vis. Sci. *41*, 4069–4073.

26. Guillonneau, X., Piriev, N.I., Danciger, M., Kozak, C.A., Cideciyan, A.V., Jacobson, S.G., and Farber, D.B. (1999). A nonsense mutation in a novel gene is associated with retinitis pigmentosa in a family linked to the RP1 locus. Hum. Mol. Genet. *8*, 1541–1546. https://doi.org/10.1093/hmg/8.8.1541.

27. Vandenberghe, L.H., Bell, P., Maguire, A.M., Cearley, C.N., Xiao, R., Calcedo, R., Wang, L., Castle, M.J., Maguire, A.C., Grant, R., et al. (2011). Dosage thresholds for AAV2 and AAV8 photoreceptor gene therapy in monkey. Sci. Transl. Med. *3*, 88ra54. https://doi.org/10.1126/scitranslmed.3002103.

28. Ramachandran, P.S., Lee, V., Wei, Z., Song, J.Y., Casal, G., Cronin, T., Willett, K., Huckfeldt, R., Morgan, J.I.W., Aleman, T.S., et al. (2017). Evaluation of dose and safety of AAV7m8 and AAV8BP2 in the non-human primate retina. Hum. Gene Ther. *28*, 154–167. https://doi.org/10.1089/hum.2016.111.

29. Khabou, H., Cordeau, C., Pacot, L., Fisson, S., and Dalkara, D. (2018). Dosage thresholds and influence of transgene cassette in adeno-associated virus-related toxicity. Hum. Gene Ther. *29*, 1235–1241. https://doi.org/10.1089/hum.2018.144.

30. Mingozzi, F., and High, K.A. (2013). Immune responses to AAV vectors: overcoming barriers to successful gene therapy. Blood *122*, 23–36. https://doi.org/10.1182/blood-2013-01-306647.

31. Pryadkina, M., Lostal, W., Bourg, N., Charton, K., Roudaut, C., Hirsch, M.L., and Richard, I. (2015). A comparison of AAV strategies distinguishes overlapping vectors for efficient systemic delivery of the 6.2 kb Dysferlin coding sequence. Mol. Ther. Methods Clin. Dev. *2*, 15009. https://doi.org/10.1038/mtm.2015.9.

32. Dong, B., Nakai, H., and Xiao, W. (2010). Characterization of genome integrity for oversized recombinant AAV vector. Mol. Ther. *18*, 87–92. https://doi.org/10.1038/mt.2009.258.

33. Nakai, H., Storm, T.A., and Kay, M.A. (2000). Recruitment of single-stranded recombinant adeno-associated virus vector genomes and intermolecular recombination are responsible for stable transduction of liver in vivo. J. Virol. *74*, 9451–9463. https://doi.org/10.1128/jvi.74.20.9451-9463.2000.

34. Hirsch, M.L., Li, C., Bellon, I., Yin, C., Chavala, S., Pryadkina, M., Richard, I., and Samulski, R.J. (2013). Oversized AAV transductifon is mediated via a DNA-PKcs-independent, Rad51C-dependent repair pathway. Mol. Ther. *21*, 2205–2216. https://doi.org/10.1038/mt.2013.184.

35. Halbert, C.L., Allen, J.M., and Miller, A.D. (2002). Efficient mouse airway transduction following recombination between AAV vectors carrying parts of a larger gene. Nat. Biotechnol. *20*, 697–701. https://doi.org/10.1038/nbt0702-697.

36. Tran, N.T., Heiner, C., Weber, K., Weiand, M., Wilmot, D., Xie, J., Wang, D., Brown, A., Manokaran, S., Su, Q., et al. (2020). AAV-genome population sequencing of vectors packaging CRISPR components reveals design-influenced heterogeneity. Mol. Ther. Methods Clin. Dev. *18*, 639–651. https://doi.org/10.1016/j.omtm.2020.07.007.

37. Yang, J., Zhou, W., Zhang, Y., Zidon, T., Ritchie, T., and Engelhardt, J.F. (1999). Concatamerization of adeno-associated virus circular genomes occurs through intermolecular recombination. J. Virol. *73*, 9468–9477. https://doi.org/10.1128/jvi.73.11.9468-9477.1999.

38. Reich, S.J., Auricchio, A., Hildinger, M., Glover, E., Maguire, A.M., Wilson, J.M., and Bennett, J. (2003). Efficient trans-splicing in the retina expands the utility of adeno-associated virus as a vector for gene therapy. Hum. Gene Ther. *14*, 37–44. https://doi.org/10.1089/10430340360464697.

39. Duan, D., Yue, Y., and Engelhardt, J.F. (2001). Expanding AAV packaging capacity with trans-splicing or overlapping vectors: a quantitative comparison. Mol. Ther. *4*, 383–391. https://doi.org/10.1006/mthe.2001.0456.

40. Trapani, I., Colella, P., Sommella, A., Iodice, C., Cesi, G., de Simone, S., Marrocco, E., Rossi, S., Giunti, M., Palfi, A., et al. (2014). Effective delivery of large genes to the retina by dual AAV vectors. EMBO Mol. Med. *6*, 194–211. https://doi.org/10.1002/emmm.201302948.

41. Duan, D., Yue, Y., Yan, Z., and Engelhardt, J.F. (2000). A new dual-vector approach to enhance recombinant adeno-associated virus-mediated gene expression through intermolecular cis activation. Nat. Med. *6*, 595–598. https://doi.org/10.1038/75080.

42. Ghosh, A., Yue, Y., Lai, Y., and Duan, D. (2008). A hybrid vector system expands adeno-associated viral vector packaging capacity in a transgene-independent manner. Mol. Ther. *16*, 124–130. https://doi.org/10.1038/sj.mt.6300322.

43. Flotte, T.R., Afione, S.A., Solow, R., Drumm, M.L., Markakis, D., Guggino, W.B., Zeitlin, P.L., and Carter, B.J. (1993). Expression of the cystic fibrosis transmembrane conductance regulator from a novel adeno-associated virus promoter. J. Biol. Chem. *268*, 3781–3790.

44. Earley, L.F., Conatser, L.M., Lue, V.M., Dobbins, A.L., Li, C., Hirsch, M.L., and Samulski, R.J. (2020). Adeno-associated virus serotype-specific inverted terminal repeat sequence role in vector transgene expression. Hum. Gene Ther. *31*, 151–162. https://doi.org/10.1089/hum.2019.274.

45. Fujita, K., Nishiguchi, K.M., Yokoyama, Y., Tomiyama, Y., Tsuda, S., Yasuda, M., Maekawa, S., and Nakazawa, T. (2015). In vivo cellular imaging of various stress/response pathways using AAV following axonal injury in mice. Sci. Rep. *5*, 18141. https://doi.org/10.1038/srep18141.

46. Nagai, T., Ibata, K., Park, E.S., Kubota, M., Mikoshiba, K., and Miyawaki, A. (2002). A variant of yellow fluorescent protein with fast and efficient maturation for cell-biological applications. Nat. Biotechnol. *20*, 87–90. https://doi.org/10.1038/nbt0102-87.

47. Fujita, K., Nishiguchi, K.M., Shiga, Y., and Nakazawa, T. (2017). Spatially and temporally regulated NRF2 gene therapy using Mcp-1 promoter in retinal ganglion cell injury. Mol. Ther. Methods Clin. Dev. *5*, 130–141. https://doi.org/10.1016/j.omtm.2017.04.003.

48. Li, H. (2018). Minimap2: pairwise alignment for nucleotide sequences. Bioinformatics *34*, 3094–3100. https://doi.org/10.1093/bioinformatics/bty191.

49. Li, H. (2021). New strategies to improve minimap2 alignment accuracy. Bioinformatics *37*, 4572–4574. https://doi.org/10.1093/bioinformatics/btab705.

50. Robinson, J.T., Thorvaldsdóttir, H., Winckler, W., Guttman, M., Lander, E.S., Getz, G., and Mesirov, J.P. (2011). Integrative genomics viewer. Nat. Biotechnol. *29*, 24–26. https://doi.org/10.1038/nbt.1754.

51. Thorvaldsdóttir, H., Robinson, J.T., and Mesirov, J.P. (2013). Integrative Genomics Viewer (IGV): high-performance genomics data visualization and exploration. Brief. Bioinform. *14*, 178–192. https://doi.org/10.1093/bib/bbs017.

52. Robinson, J.T., Thorvaldsdóttir, H., Wenger, A.M., Zehir, A., and Mesirov, J.P. (2017). Variant review with the Integrative Genomics Viewer. Cancer Res. *77*, e31–e34. https://doi.org/10.1158/0008-5472.can-17-0337.

53. Robinson, J.T., Thorvaldsdottir, H., Turner, D., and Mesirov, J.P. (2023). igv.js: an embeddable JavaScript implementation of the Integrative Genomics Viewer (IGV). Bioinformatics *39*, btac830. https://doi.org/10.1093/bioinformatics/btac830.

54. Yamada, K., Tazaki, A., Ushio-Watanabe, N., Usui, Y., Takeda, A., Matsunaga, M., Suzumura, A., Shimizu, H., Zheng, H., Ariefta, N.R., et al. (2023). Retinal ferroptosis as a critical mechanism for the induction of retinochoroiditis during ocular toxoplasmosis. Redox Biol. *67*, 102890. https://doi.org/10.1016/j.redox.2023.102890.

55. Maeder, M.L., Stefanidakis, M., Wilson, C.J., Baral, R., Barrera, L.A., Bounoutas, G. S., Bumcrot, D., Chao, H., Ciulla, D.M., DaSilva, J.A., et al. (2019). Development of a gene-editing approach to restore vision loss in Leber congenital amaurosis type 10. Nat. Med. *25*, 229–233. https://doi.org/10.1038/s41591-018-0327-9.